

Proximity-induced superconductivity within the InAs/GaSb edge conducting state.

A. Kononov,¹ V.A. Kostarev,¹ B.R. Semyagin,² V.V. Preobrazhenskii,²
M.A. Putyato,² E.A. Emelyanov,² and E.V. Deviatov¹

¹*Institute of Solid State Physics RAS, 142432 Chernogolovka, Russia*

²*Institute of Semiconductor Physics, Novosibirsk 630090, Russia*

(Dated: March 8, 2024)

We experimentally investigate Andreev transport through the interface between an indium superconductor and the edge of the InAs/GaSb bilayer. To cover all possible regimes of InAs/GaSb spectrum, we study samples with 10-nm, 12 nm, and 14 nm thick InAs quantum wells. For the trivial case of a direct band insulator in 10 nm samples, differential resistance demonstrates standard Andreev reflection. For InAs/GaSb structures with band inversion (12 nm and 14 nm samples), we observe distinct low-energy structures, which we regard as direct evidence for the proximity-induced superconductivity within the current-carrying edge state. For 14 nm InAs well samples, we additionally observe mesoscopic-like resistance fluctuations, which are subjected to threshold suppression in low magnetic fields.

PACS numbers: 73.40.Qv 71.30.+h

I. INTRODUCTION

Similarly to HgTe quantum wells^{1,2}, InAs/GaSb bilayers can demonstrate inverted energy spectra³. For a typical value of 10 nm for the GaSb layer, InAs/GaSb structures with 12 nm thick InAs wells are usually regarded as topological insulators³⁻⁸. Thinner (10 nm) or thicker (14 nm) InAs wells correspond^{8,9} to a direct band semiconductor or an indirect band two-dimensional semimetal, respectively. InAs/GaSb bilayers possess many advantages over HgTe quantum wells, including better stability, much easier III-V materials processing and spectra tunability by front and back gates³. However, there is residual bulk conductivity in InAs/GaSb structures, which complicates experimental investigation of edge transport^{8,10}.

Topological edge states with spin-momentum locking are expected for structures with band inversion¹¹⁻¹⁴. Current-carrying edge states were demonstrated for InAs/GaSb bilayers in transport experiments^{6,8,10,15,16}, although their topological nature is still debatable¹⁶.

Edge state transport is of special interest for regions with proximity-induced superconductivity¹⁷⁻¹⁹, because of a search for Majorana fermions with non-Abelian statistics²⁰ and prospects for quantum computing^{19,21}. This activity requires detailed investigation of Andreev transport in systems with non-trivial energy spectra²²⁻²⁴.

Andreev reflection²⁵ allows charge transport from normal metal (N) to superconductor (S) at energies below the superconducting gap. An electron is injected through the NS interface by creating a Cooper pair, so a hole is reflected back to the N side of the junction^{25,26}. Usually, Andreev reflection is not sensitive to the details of band structure in the normal lead²⁶. However, for graphene or semimetal spectra, the reflected hole can appear in the valence band, which is known as specular (or interband) Andreev reflection²⁷⁻²⁹. Also, an additional energy scale appears if Andreev transport goes through an intermediate conductive region, which is partially decoupled from

the bulk normal conductor^{30,31}.

Here, we experimentally investigate Andreev transport through the interface between an indium superconductor and the edge of the InAs/GaSb bilayer. To cover all possible regimes of InAs/GaSb spectrum, we study samples with 10-nm, 12 nm, and 14 nm thick InAs quantum wells. For the trivial case of a direct band insulator in 10 nm samples, differential resistance demonstrates standard Andreev reflection. For InAs/GaSb structures with band inversion (12 nm and 14 nm samples), we observe distinct low-energy structures, which we regard as direct evidence for the proximity-induced superconductivity within the current-carrying edge state. For 14 nm InAs well samples, we additionally observe mesoscopic-like resistance fluctuations, which are subjected to threshold suppression in low magnetic fields.

II. SAMPLES AND TECHNIQUE

Our samples are grown by solid source molecular beam epitaxy on semi-insulating GaAs (100) substrate. The InAs/GaSb double quantum well is sandwiched between two 50 nm thick AlSb barriers. Details on the growth parameters can be found elsewhere³². To cover all possible regimes of the InAs/GaSb bilayer spectrum^{8,9}, we prepare samples with a 10-nm thick GaSb quantum well and different, 10-nm, 12 nm, and 14 nm thick InAs ones, see Fig. 1.

As obtained from standard magnetoresistance measurements, the 10 nm and 14 nm samples are characterized by bulk electron-type conductivity, while it is hole-type for the 12 nm ones. The low-temperature mobility is found to be one order of magnitude higher for bulk electrons (10^4 cm²/Vs) than for holes (10^3 cm²/Vs). These values are in good correspondence with known ones for InAs/GaSb double quantum wells³⁻⁷, taking into account low bulk carrier concentration, which is roughly $\approx 4 \cdot 10^{11}$ cm⁻² in all our samples.

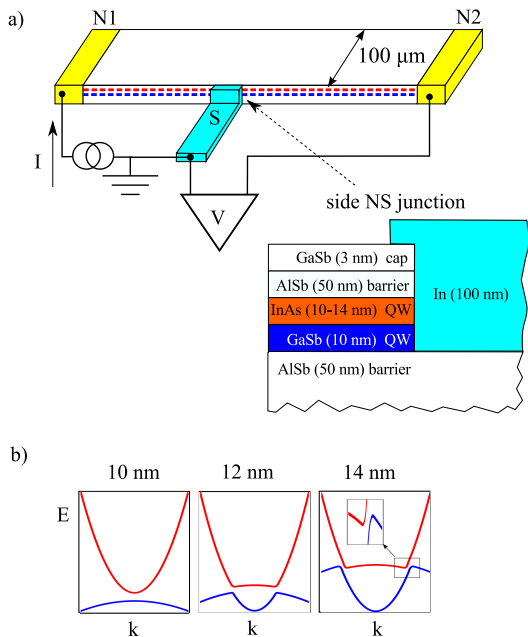


FIG. 1. (Color online) (a) Sketch of the sample (not to scale) with electrical connections. $10\ \mu\text{m}$ wide side normal-superconductor In–InAs/GaSb junctions are fabricated by lift-off technique, after thermal evaporation of a thick In film (gray) over the mesa step. Charge transport is investigated across a single In–InAs/GaSb junction in a standard three-point technique: the superconducting electrode is grounded, while Ohmic contacts N1 and N2 (yellow) are employed to feed the current and measure the voltage drop, respectively. (b) Schematic diagrams of the expected energy spectrum for different InAs quantum well thicknesses, see Refs. 8 and 9 for details.

A sample sketch is presented in Fig. 1 (a). The $80\ \text{nm}$ high mesa is formed by wet chemical etching down to the bottom GaSb layer. Since the edge effects are of prime interest in InAs/GaSb bilayers^{3–7}, side^{33,34} superconducting contacts are made at the mesa step. They are formed from thermally evaporated $100\ \text{nm}$ thick indium film by lift-off with low ($1\text{--}2\ \mu\text{m}$) mesa overlap, see Fig. 1 (a). Because of the insulating top AlSb barrier, vertical transport is forbidden in the overlap region. We take special care to obtain equally prepared In–InAs/GaSb interfaces. Both the processing steps, wet etching and indium evaporation, are made simultaneously for samples with 10-nm , $12\ \text{nm}$, and $14\ \text{nm}$ thick InAs quantum wells. Ohmic contacts are made by thermal evaporation of $100\ \text{nm}$ Au film with few nm Ni to improve adhesion.

We study charge transport across a single NS junction between the indium side contact and the InAs/GaSb mesa edge in a standard three-point technique, see Fig. 1 (a): the superconducting electrode is grounded; a current (-2 to $+2\ \mu\text{A}$ range) is fed to InAs/GaSb bilayer through one of the normal Ohmic contacts, N1 in Fig. 1; the other normal contact (N2, respectively) traces the potential V .

To obtain $dV/dI(V)$ characteristics, the current is additionally modulated by a low ac ($20\ \text{pA}$, $110\ \text{Hz}$) com-

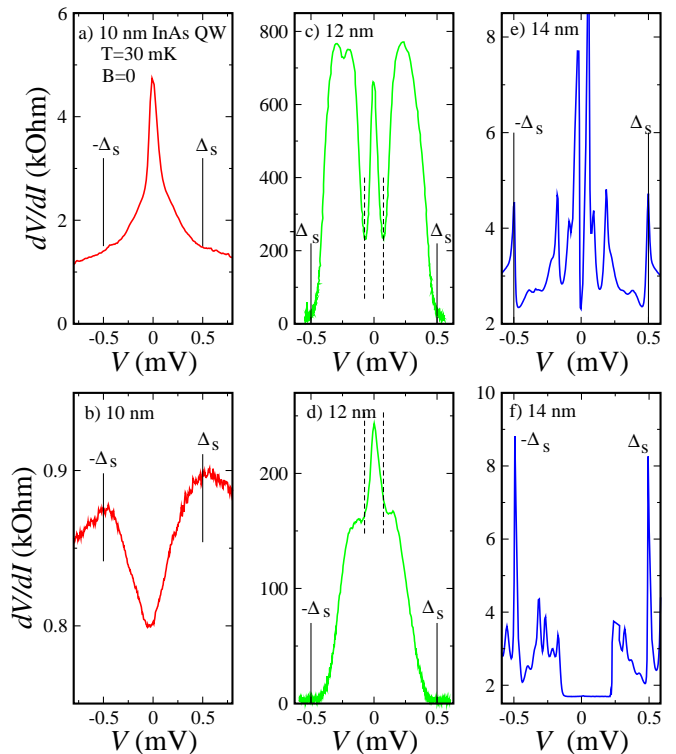


FIG. 2. (Color online) $dV/dI(V)$ curves for a single In–InAs/GaSb junction for different samples. For every curve, dV/dI is finite within the indium superconducting gap $|eV| < \Delta_s = 0.5\ \text{meV}$ due to Andreev reflection. The top and the bottom panels demonstrate maximum device-to-device fluctuations for a given InAs quantum well thickness: (a–b) $10\ \text{nm}$, which is expected to have trivial insulator band structure. There is no any additional dV/dI features; (c–d) $12\ \text{nm}$, a supposed topological insulator. There is well-developed dV/dI peak within $\pm 0.07\ \text{mV}$, the subgap dV/dI resistance is extremely high, about $200\text{--}800\ \text{kOhm}$; (e–f) $14\ \text{nm}$, two-dimensional indirect-band semimetal. A zero-bias resistance dip is accompanied by a number of additional symmetric peaks of different amplitude. The curves are obtained at $30\ \text{mK}$ in zero magnetic field.

ponent. We measure both, dc (V) and ac ($\sim dV/dI$), components of the potential by using a dc voltmeter and a lock-in, respectively. We check, that the lock-in signal is independent of the modulation frequency in the $60\ \text{Hz}\text{--}300\ \text{Hz}$ range, which is defined by applied ac filters. To extract features specific to the InAs/GaSb bilayer system, the measurements are performed at $30\ \text{mK}$. Similar results are obtained from different samples in several cooling cycles.

III. EXPERIMENTAL RESULTS

Fig. 2 demonstrates examples of $dV/dI(V)$ curves for samples with different thickness of InAs quantum well. In a three-point technique, the measured potential V reflects in-series connected resistances of the grounded con-

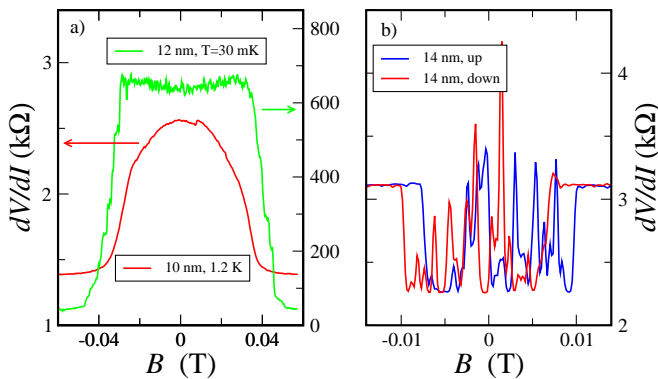


FIG. 3. (Color online) (a) Suppression of the superconductivity by in-plane magnetic field for the 10 nm sample at 1.2 K and for the 12 nm one at 30 mK. The resistance drop is clearly broadened at high temperature. Monotonous $dV/dI(B)$ suppression is fully consistent with the classical Andreev reflection picture²⁶. (b) Threshold suppression of the mesoscopic-like resistance fluctuations by low in-plane magnetic field for the 14 nm sample at 30 mK. The exact threshold positions depend slightly on the magnetic field direction. The dc bias is fixed at $V = 0$ during the field sweep.

tact and some part of the 2D system. In our experiment the former term is dominant, because of highly resistive junctions, see Fig. 2. The indium lead is superconducting, so $dV/dI(V)$ characteristics reflect charge transport through a single (grounded) NS interface. To support this conclusion experimentally, the obtained $I - V$ characteristics are verified to be independent of the exact positions of current and voltage probes.

Despite of equally prepared In-InAs/GaSb interfaces, $dV/dI(V)$ curves demonstrate even qualitative different behavior in samples with different thickness of InAs quantum well in Fig. 2. Since the $dV/dI(V)$ curves of NS junctions are known to be highly sensitive to the interface potential fluctuations³⁵, the top and the bottom panels in Fig. 2 demonstrate maximum device-to-device fluctuations for a given InAs quantum well thickness.

The 10 nm wide InAs quantum well sample demonstrates a typical example of Andreev reflection at the disordered NS interface²⁶, see Fig. 2 (a-b). In (a), the differential resistance dV/dI is increased within the indium superconducting gap $|eV| < \Delta_s = 0.5$ meV to about 5 k Ω , so single-particle scattering is significant at the interface³⁵. In Fig. 2 (b), there is a resistance drop within $|eV| < \Delta_s = 0.5$ meV, as it is expected for cleaner NS interface^{25,35}. There is no any additional dV/dI features for the curves in Fig. 2 (a-b), as it should be anticipated for standard Andreev reflection.

In Fig. 2 (c-d), the subgap dV/dI resistance is about $200 - 800$ k Ω in different samples at $|eV| < \Delta_s = 0.5$ meV. It is much higher than the normal dV/dI value ≈ 20 k Ω for $|eV| > \Delta_s$. Which is specific for the 12 nm samples, there is always well-developed dV/dI peak within ± 0.07 mV bias.

The $dV/dI(V)$ behavior is even more complicated for

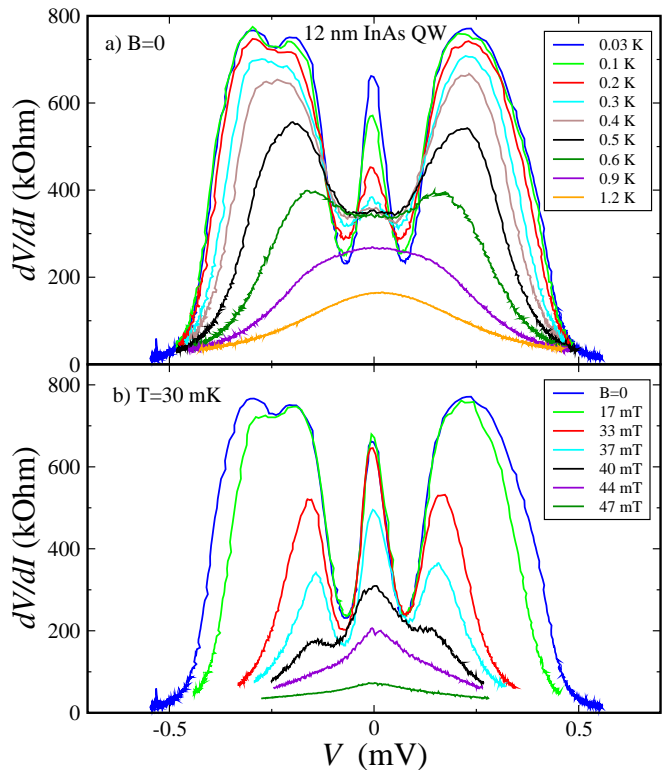


FIG. 4. (Color online) $dV/dI(V)$ behavior with temperature (a) or magnetic field (b) for the 12 nm sample. The superconductivity is gradually suppressed, but the resistance peak within ± 0.07 mV is well visible for temperatures below 0.6 K in zero field (a) and below 40 mT at minimal temperature (b).

the 14 nm samples, see Fig. 2 (e-f). Differential resistance demonstrates sharp peaks at $|eV| = \Delta_s$, the sub-gap and normal dV/dI values are comparable with the 10 nm case. However, a zero-bias resistance dip appears in Fig. 2 (e-f), which is accompanied by a number of additional resistance peaks of different amplitude. They are well reproducible for a given sample and symmetric in respect to the bias sign.

First of all, we demonstrate that the presented in Fig. 2 $dV/dI(V)$ curves are connected with superconductivity. Fig. 3 (a) demonstrates that the superconductivity can be completely suppressed above ≈ 30 mT, which well corresponds to the known³⁶ bulk indium critical field. We fix the zero bias $V = 0$ and sweep the magnetic field slowly. The resistance drop is sharp at 30 mK (as shown for the 12 nm sample), while temperature broadening is demonstrated at 1.2 K for the 10 nm sample in Fig. 3. To avoid orbital effects, the field is oriented within the bilayer plane (with 0.5° accuracy) along the mesa edge, so it is strictly in-plane oriented also for the superconducting film at the mesa step. We obtain similar results for the normally oriented magnetic field. Monotonous $dV/dI(B)$ suppression is fully consistent with the classical Andreev reflection picture²⁶.

Fig. 3 (b) demonstrates specifics of the low-field be-

havior for the 14 nm samples. One can see strong mesoscopic-like $dV/dI(B)$ fluctuations within $\approx \pm 10mT$ interval, which are completely suppressed at higher fields.

Fig. 4 demonstrates detailed $dV/dI(V)$ behavior with temperature or magnetic field increase for the 12 nm sample. The resistance peak within ± 0.07 mV is well visible for temperatures below 0.6 K, see Fig. 4 (a), and for magnetic fields below 40 mT in Fig. 4 (b). At the temperature of 1.2 K, $dV/dI(V)$ curve is still nonlinear because of much higher indium $T_c \approx 3.4$ K. The superconductivity is gradually suppressed above 30 mT in Fig. 4 (b), further increase of magnetic field results in a nearly flat curve even at lowest $T = 30$ mK.

IV. DISCUSSION

Within the classical framework of Andreev reflection²⁶, it is not sensitive to details of band structure in a normal lead. However, even qualitative effect on $dV/dI(V)$ can be seen in Fig. 2 for samples with different InAs quantum well widths. Because the observed subgap features are independent of the maximum device-to-device fluctuations, we have to attribute them to different edge properties of our InAs/GaSb structures, which are defined by bulk spectrum³⁻⁷.

No edge specifics can be expected for a trivial insulator in 10 nm thick InAs quantum well samples. Monotonous $dV/dI(V)$ curves in Fig. 2 (a-b) do not demonstrate subgap features, they are only sensitive to the disorder at the interface³⁵.

In the case of 12 nm thick InAs quantum well, the current-carrying edge states appear, because of the inverted band structure. This statement seems to be firmly confirmed by experiments³⁻⁷. Moreover, the edge current was directly demonstrated in visualization experiments^{6,37} to coexist with finite bulk conductivity, most likely due to the edge depletion region. The latter leads to strongly increased differential resistance in Fig. 2 (c-d). The proximity-induced superconducting gap Δ_{ind} can be expected within the edge state near the indium superconducting lead²².

Andreev transport through the intermediate conductive region has been regarded both experimentally^{30,31} and theoretically³⁸. In a crude qualitative picture, see Fig. 5, the NS' interface with the region of induced superconductivity S' is responsible for Andreev reflection at biases below the induced gap $|eV| < \Delta_{ind}$, while above this value the NS interface with bulk superconductor governs the reflection process. Because of different single-particle transparency of two interfaces, $dV/dI(V)$ contains^{30,31} an additional structure at low biases. The induced gap Δ_{ind} can be estimated from the width of this structure^{30,31} in Fig. 2 (c-d) as 0.07 meV.

Because the edge conductive region is of finite width^{6,37} L , the induced gap should be defined by Thouless energy $\Delta_{ind} \sim E_{Th}$ (see Appendix to Ref. 38 for recent comprehensive discussion). This statement is in

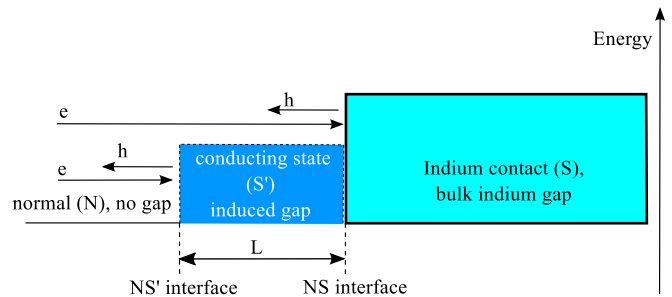


FIG. 5. (Color online) Schematic energy diagram of the edge region for InAs/GaSb structures with band inversion. The proximity-induced superconductivity (blue region S') can be expected within the conductive edge state near the indium superconducting lead²². The NS' interface is responsible for Andreev reflection at biases below the induced gap $|eV| < \Delta_{ind}$, while above this value the NS interface with bulk superconductor (S) governs the reflection process. Because of different single-particle transparency of the interfaces, $dV/dI(V)$ contains³¹ an additional structure at low biases in Fig. 2 (c-d) and (e-f)

qualitative agreement with our experiment: (i) as expected³⁹ for E_{Th} , the width of the low-bias structure is constant in Fig. 4 (a), until $k_B T$ exceeds Δ_{ind} at 0.9 K; (ii) also, E_{Th} is insensitive³⁹ to partial suppression of the bulk superconducting gap by magnetic field, as we observe in Fig. 4 (b). As for numerical estimations, $E_{Th} = \hbar D/L^2$ in the regime of diffusive transport. If we use the bulk values, $v_F \approx 6 \times 10^4$ m/s and $l \approx 10$ nm, we can estimate L as 60 nm from the experimental value of $E_{Th} \approx 0.07$ meV. This crude estimation corresponds well to the experimentally obtained¹⁵ value $L < 260$ nm.

Because of the band inversion, we can also expect⁹ the edge conductive region for samples with 14 nm width of the InAs quantum well. Thus, the zero-bias resistance dip in Fig. 2 (e-f) can also be regarded as the induced gap $\Delta_{ind} \sim E_{Th}$. However, the subgap resistance peaks in Fig. 2 (e-f) and mesoscopic-like fluctuations in low fields in Fig. 3 (b) resemble modulation^{38,41} of density of states due to the quasiparticle interference³⁸. It appears^{22,42} for ballistic $l \gg L$ transport, which seems to be reasonable for $l \approx 100$ nm in the 14 nm samples. In this case, the threshold suppression of the mesoscopic-like fluctuations reflects the interference breakdown in magnetic field. It is important, that we do not observe any subgap features for the 10 nm samples with the similar $l \approx 100$ nm value, where no edge conductive region can be expected. Thus, we can regard the subgap resistance features in Fig. 2 (c-d) and (e-f) as a direct evidence for the proximity-induced superconductivity within the current-carrying edge states in InAs/GaSb structures with band inversion.

V. CONCLUSION

As a conclusion, we experimentally investigate Andreev transport through the interface between an indium superconductor and the edge of the InAs/GaSb bilayer. To cover all possible regimes of InAs/GaSb spectrum, we study samples with 10-nm, 12 nm, and 14 nm thick InAs quantum wells. For the trivial case of a direct band insulator in 10 nm samples, differential resistance demonstrates standard Andreev reflection. For InAs/GaSb structures with band inversion (12 nm and 14 nm samples), we observe distinct low-energy structures, which we

regard as direct evidence for the proximity-induced superconductivity within the current-carrying edge state. For 14 nm InAs well samples, we additionally observe mesoscopic-like resistance fluctuations, which are subjected to threshold suppression in low magnetic fields.

ACKNOWLEDGMENTS

We wish to thank Ya. Fominov, D.E. Feldman, V.T. Dolgoplov, and T.M. Klapwijk for fruitful discussions. We gratefully acknowledge financial support by the RFBR (project No. 16-02-00405) and RAS.

-
- ¹ M. König, S. Wiedmann, C. Brune, A. Roth, H. Buhmann, L.W. Molenkamp, X.-L. Qi, and S.-C. Zhang, *Science* **318**, 766 (2007).
- ² G. M. Gusev, Z. D. Kvon, O. A. Shegai et al. , *Phys. Rev. B* **84**, 121302(R) (2011).
- ³ C. Liu, T.L. Hughes, X.-L. Qi, K. Wang, and S.-C. Zhang, *Phys. Rev. Lett.* **100**, 236601 (2008).
- ⁴ I. Knez, R.-R. Du, and G. Sullivan, *Phys. Rev. Lett.* **107**, 136603 (2011).
- ⁵ I. Knez, C. T. Rettner, S.-H. Yang, S. S. P. Parkin, L. Du, R.-R. Du, and G. Sullivan, *Phys. Rev. Lett.* **112**, 026602 (2014).
- ⁶ E.M. Spanton, K.C. Nowack, L. Du, G. Sullivan, R.-R. Du, K.A. Moler, *Phys. Rev. Lett.* **113**, 026804 (2014).
- ⁷ L. Du, I. Knez, G. Sullivan, and R.-R. Du, *Phys. Rev. Lett.* **114**, 096802 (2015).
- ⁸ K. Suzuki, Y. Harada, K. Onomitsu, and K. Muraki, *Phys. Rev. B* **87**, 235311 (2013).
- ⁹ L. Tiemann, S. Mueller, Q.-S. Wu, T. Tschirky, K. Ensslin, W. Wegscheider, M. Troyer, A.A. Soluyanov, and T. Ihn, *Phys. Rev. B* **95**, 115108 (2017).
- ¹⁰ L. Du, I. Knez, G. Sullivan, R.-R. Du, *Phys. Rev. Lett.* **114**, 096802 (2015).
- ¹¹ S. Murakami, N. Nagaosa, S.-C. Zhang, *Phys. Rev. Lett.* **93**, 156804 (2004).
- ¹² C. L. Kane, E. J. Mele, *Phys. Rev. Lett.* **95**, 146802 (2005).
- ¹³ B. A. Bernevig, S.-C. Zhang, *Phys. Rev. Lett.* **96**, 106802 (2006).
- ¹⁴ Y. Ando, *J. Phys. Soc. Jpn.* **82**, 102001 (2013).
- ¹⁵ V.S. Pribiag, A.J.A. Beukman, F. Qu, M.C. Cassidy, C. Charpentier, W. Wegscheider and L.P. Kouwenhoven, *Nature Nanotechnology* **10**, 593597 (2015).
- ¹⁶ F. Nichele, H.J. Suominen, M. Kjaergaard, C.M. Marcus, E. Sajadi, J.A. Folk, F. Qu, A.J.A. Beukman, F.K. de Vries, J. van Veen, S. Nadj-Perge, L.P. Kouwenhoven, B.-M. Nguyen, A.A. Kiselev, W. Yi, M. Sokolich, M.J. Manfra, E.M. Spanton and K.A. Moler, *New J. Phys.* **18**, 083005 (2016).
- ¹⁷ L. Fu and C. L. Kane, *Phys. Rev. Lett.* **100**, 96407 (2008).
- ¹⁸ S. Hart, H. Ren, T. Wagner, Ph. Leubner, M. Mühlbauer, C. Brüne, H. Buhmann, L. W. Molenkamp and A. Yacoby, *Nature Physics* **10**, 638643 (2014).
- ¹⁹ C.W.J. Beenakker, *Annu. Rev. Con. Mat. Phys.* **4**, 113 (2013).
- ²⁰ For recent reviews, see C. W. J. Beenakker, *Annu. Rev. Con. Mat. Phys.* **4**, 113 (2013) and J. Alicea, *Rep. Prog. Phys.* **75**, 076501 (2012).
- ²¹ S.B. Bravyi and A.Y. Kitaev, *Annals of Physics* **298**, 210 (2002).
- ²² P. Adroguer, C. Grenier, D. Carpentier, J. Cayssol, P. Degiovanni, and E. Orignac, *Phys. Rev. B* **82**, 081303(R), (2010).
- ²³ C. Visani, Z. Sefrioui, J. Tornos, C. Leon, J. Briatico, M. Bibes, A. Barthelemy, J. Santamara and Javier E. Villegas, *Nature Physics*, **8**, 539 (2012).
- ²⁴ A.D.K. Finck, C. Kurter, Y.S. Hor, D.J. Van Harlingen, *Phys. Rev. X* **4**, 041022 (2014).
- ²⁵ A. F. Andreev, *Soviet Physics JETP* **19**, 1228 (1964).
- ²⁶ M. Tinkham, *Introduction to Superconductivity* (2d ed., McGrawHill, New York, 1996).
- ²⁷ C. W. J. Beenakker, *Physical Review Letters* **97** (2006).
- ²⁸ C. W. J. Beenakker, *Reviews of Modern Physics* **80**, 1337 (2008).
- ²⁹ Wei Chen, Liang Jiang, R. Shen, L. Sheng, B. G. Wang, D. Y. Xing *EPL* **103**, 27006 (2013)
- ³⁰ D.R. Heslinga, S.E. Shafranjuk, H. van Kempen, and T.M. Klapwijk, *Phys. Rev. B* **49**, 10484 (1994).
- ³¹ J. Wiedenmann, E. Liebhaber, J.s Kübert, E. Bocquillon, Ch. Ames, H. Buhmann, T.M. Klapwijk, L.W. Molenkamp, arXiv:1706.01638.
- ³² E.A. Emelyanov, D.F. Feklin, A.V. Vasev, M.A. Putyato, B.R. Semyagin, A.P. Vasilenko, O.P. Pchelyakov, V.V. Preobrazhenskii, *Optoelectronics, Instrumentation and Data Processing*, **47**, 452 (2011).
- ³³ A. Kononov, S. V. Egorov, Z. D. Kvon, N. N. Mikhailov, S. A. Dvoretzky, and E. V. Deviatov, *Phys. Rev. B* **93**, 041303(R) (2016)
- ³⁴ A. Kononov, S. V. Egorov, N. Titova, Z. D. Kvon, N. N. Mikhailov, S. A. Dvoretzky, E. V. Deviatov, *JETP Lett.*, **101**, 41 (2015).
- ³⁵ G.E. Blonder, M. Tinkham, T.M. Klapwijk, *Physical Review B*, **25**, 4515 (1982).
- ³⁶ A. M. Toxen *Phys. Rev.* **123**, 442 (1961)
- ³⁷ K.C. Nowack, E.M. Spanton, M. Baenninger, et al., *Nature Materials* **12**, 787 (2013).
- ³⁸ T.Ö. Rosdahl, A. Vuik, M. Kjaergaard, A.R. Akhmerov, arXiv:1706.08888v1.
- ³⁹ M. Snelder, M.P. Stehno, A.A. Golubov, C.G. Molenaar, T. Scholten, D. Wu, Y.K. Huang, W.G. van der Wiel,

M.S. Golden, and A. Brinkman, arXiv:1506.05923.

⁴⁰ D.I. Pikulin and T. Hyart, Phys. Rev. Lett. **112**, 176403 (2014).

⁴¹ D. Chevallier, P. Simon, and C. Bena, Phys. Rev. B **88**, 165401 (2013).

⁴² W. J. Tomasch, Phys. Rev. Lett. **16**, 16 (1966).